Title

Automated Detection and Analysis of Foraging Behavior in C. elegans

Authors

Huang, K.-M.
Cosman, P
Schafer, W R

Publication Date

2008-03-01

Peer reviewed

Automated Detection and Analysis of Foraging Behavior in *C. elegans*

Kuang-Man Huang, Pamela Cosman,
Electrical and Computer Engineering
University of California at San Diego
La Jolla, CA, 92093-0407, USA.

William R. Schafer
Cell Biology Division
MRC Laboratory of Molecular Biology
Cambridge, CB2 0QH, UK

Abstract

Foraging is a rapid, side-to-side movement of the nose generated by C. elegans as it explores its environment. We present an automated method to detect and analyze foraging behavior in a video sequence. Morphological image processing methods are used to locate the nose position of the worm in each image. Then foraging events are detected by measuring the bending angle of the nose and analyzing it with periodograms. We measure foraging-related parameters which have not previously been studied. The algorithm can be used to characterize genetic mutations associated with this behavior.

1. Introduction

The nematode *C. elegans* is useful as a neurobiological model because of its completely sequenced genome and its amenability to classical and molecular genetics. It has a compact nervous system, in which each neuron (of 302 in total) has been individually identified and characterized at the level of synaptic connectivity [1]. In principle, it is possible to identify mutants with specific behavioral abnormalities and understand mechanistically how individual gene products act within the context of the neural circuitry to produce behavioral phenotypes.

Despite its anatomically simple nervous system, *C. elegans* is capable of surprisingly diverse patterns of behaviors. While some of these, such as feeding, egg-laying, and defecation, are mechanically simple [2][3], other behaviors involve intricate coordination of muscle groups. A *C. elegans* behavior that has received comparatively little attention is foraging: rapid, side-to-side movements of the nose generated by the worm as it explores its environment. Several neurons, including the OLQ and IL1 sensory neurons and the RMG motorneurons, have been shown to be required for this behavior [4]. Various genes conferring a foraging abnormal ("Fab") phenotype have also been identified; for example, the AMPA-type glutamate receptor gene *glr-1* is required for foraging [5], and the G-protein alpha-subunit gene *goa-1* as well as other genes in the Go/Gq signaling pathway affect the rate of foraging [6]. However, the precise nature of the foraging movements in wild-type and mutant strains has not been characterized.

We provide the first quantitative description of foraging movements in *C. elegans*. Using video data collected with an automated tracking system, we detect foraging events and measure the depth and frequency of nose bends. These analyses provide more precise methods for defining the effects of specific genes and neurons on *C. elegans* behavior. In section 2, we describe the foraging detection algorithm, including image acquisition and pre-processing. In section 3, we test the algorithm on a variety of videos of mutant worms, and verify the results with manual observations. We also describe how to extract foraging-related parameters. Conclusions appear in Section 4.

2. Materials and methods

Culture methods and image acquisition: *C. elegans* strains were maintained as described [7]. For all assays, 4 day old young adults were used; fourth-stage larvae were picked the evening before the experiment and tracked the following morning. Plates used for tracking were prepared by spreading one drop of a saturated LB (Luria broth) culture of *E. coli* strain OP50 onto NGM (nematode growth medium) agar plates. Experimental animals were allowed to acclimate for 5 minutes before tracking. We used wild type worms and the following mutants: *dgk-1(nu62); glr-1(n2361); goa-1(n1143); trpa-1(ok999).*

C. elegans locomotion was tracked with a Zeiss Stemi 2000-C microscope mounted with a Cohu High Performance CCD video camera [8]. A computer-controlled tracker maintained the worms in the center of the optical field of the microscope. Image frames were captured at a frequency of 30Hz for at least one minute (30×60 = 1800 images per video). Next, we binarized the image using an adaptive threshold (the average value minus three times the standard deviation) and found the connected component with the largest

area. The original image was then trimmed to the smallest axis-aligned rectangle that contained this component, and saved as eight-bit grayscale data. The dimensions and coordinates of the rectangle were recorded. The microscope was fixed to its largest magnification (50 X) during observation. The number of pixels per millimeter was fixed at 312.5 pixel/mm.

Image pre-processing: The grayscale images were subjected to preliminary processing to generate a simplified representation of the body [8]. Images snapped when the stage was moving (the current coordinate of the stage was different from the previous coordinate) are discarded. Then for each good image frame (Figure 1a), an adaptive local thresholding algorithm followed by a morphological closing operator (binary dilation followed by erosion) was used (Figure 1b). As described in [8], a corresponding reference binary image was also generated by filling holes inside the worm body based on image content information. The difference between these two binary images provided a good indication of which image areas are worm body and which are background (Figure 1c). Following binarization, a morphological skeleton was obtained (Figure 1d) [8][9].

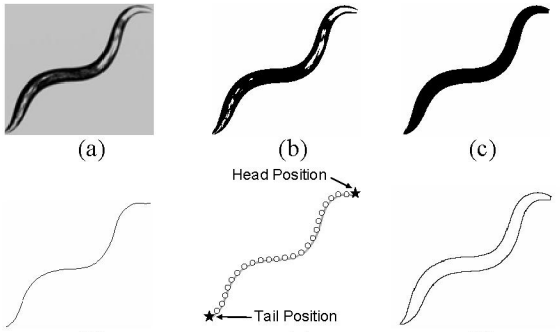

Figure 1: (a) Gray level image acquired from a video sequence. (b) Corresponding binary image after thresholding. (c) Binary image after hole filling and closing operator. (d) Skeleton after skeletonizing and pruning algorithm. (e) Skeleton with 25 sampled skeleton points. (f) The exterior contour of the worm body.

Locating the worm nose: After a morphological skeleton is obtained, the two end points on the skeleton represent the head and tail positions (Figure 1e). Using the approach in [8], the head is recognized for entire video sequences. The head is usually brighter than the tail and usually moves more than the tail. To detect foraging events which are related to subtle nose movement, we need to locate the nose position more precisely than is done in [8]. First we obtain the exterior boundary of the worm body by eroding it with a 3×3 square structuring element and performing the set difference between the binary image and its erosion (Figure 1f). Twenty-five evenly spaced points are located along the skeleton. The first two points from the head are denoted p_1 and p_2. A cutoff line is placed which passes through the point p_1 and is perpendicular to the skeleton tangent line at p_1. The cutoff line cuts the exterior contour into two parts (Figure 2a). The smaller part which contains the head point is the nose section of the contour (Figure 2b). We compute the distances between p_1 and each pixel on the nose section of the contour. The 10 points having the longest distances from p_1 are used to compute the spatial average point p_n, which we define to be the nose position (Figure 2c).

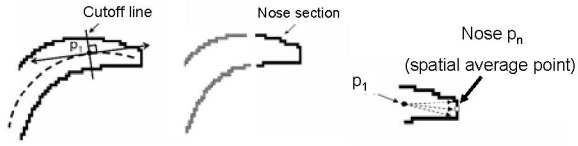

Figure 2. (a) Placing a cutoff line at the first skeleton point p_1 perpendicular to the tangent line at p_1. (b) Isolating the nose section from the rest of the body. (c) Computing the spatial average from the 10 points furthest from p_1.

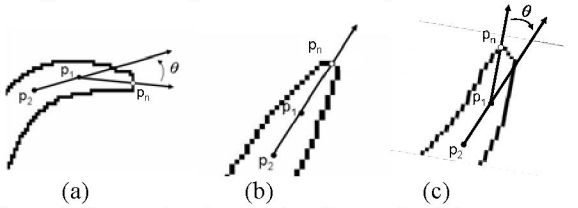

Figure 3. Computing the nose bending angle θ in every frame. (a) Nose bends to the right of midline. (b) Nose points straight ahead. (c) Nose bends to the left of midline.

Foraging event detection: In [10], a foraging movement is defined as a complete cycle of movements by the tip of the nose from the ventral side through the dorsal extreme or vice versa during time intervals when the animal was moving forward (Figure 3). Omega bends occur when the worm curves its head around to touch the middle part of its body then sharply bends away from its body. Based on the definition of foraging in [10], any detected foraging events during reversals (backward movement) or omega bends will not be counted as foraging events. We used the method in [11] to detect reversals and omega bends automatically.

To investigate this kind of side to side nose movement in a video, we measure the angle θ between the segments (p_n,p_1) and (p_1,p_2) (Figure 3). Figure 4 shows a plot of nose bending angle $b(t)$ over time from a video. Here t is the frame index. Each set of three consecutive extrema (consisting either of two local maxima and the local minimum between them, or else of two local minima and the local maximum between them) represents a side-to-side motion of the nose and

is therefore a candidate foraging event. From the beginning of each video, we examine each set of three consecutive extrema. We denote the first, second, and third local extreme values (in a time-wise order) to be the start point SP, middle point MP, and end point EP. A set of three consecutive extrema is considered to be a foraging event if that segment of the video does not contain any frames discarded due to stage movement and if either of the following two criteria is satisfied:

1) sign[SP] = sign[EP] = -sign[MP]: when this is satisfied, it means the worm's nose is waving across the midline ($\theta = 0$) to reach the other side then waving back to accomplish a complete foraging movement. An example is shown by white dots (SP_1, MP_1 and EP_1) in Fig. 4.
2) sign[SP] = sign[EP] = sign[MP] and abs[SP-MP] > α abs[SP]: when this is satisfied, it means that even though the nose does not cross the midline, its moving angle is still larger than some fraction α of its starting bending angle which, depending on α, is noticeable enough to be considered a foraging event. An example with α = 0.5 is shown by black dots (SP_2, MP_2 and EP_2) in Fig. 4. The angle difference between SP_2 and MP_2 is 15.9° which is larger than 0.5 x SP_2 =11.45°.

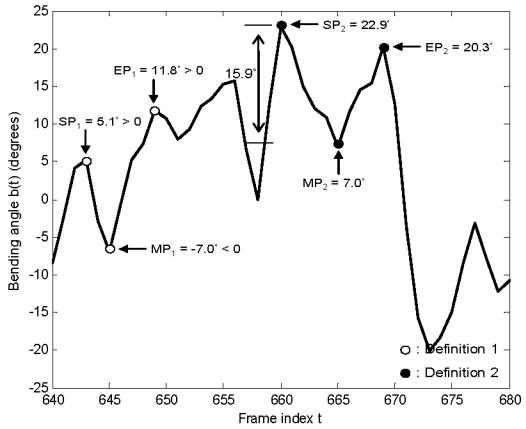

Figure 4. An example of nose bending angle over time from a video. A detected foraging event of definition 1 is shown in white dots and the other event of definition 2 (α = 0.5) is shown in black dots.

Once a set of three consecutive extrema is decided to be a foraging event, the search for additional foraging events will start from the end point EP of the previous event to avoid overlapping events.

3. Results

Verification by human observers: Our algorithm for the detection of foraging events was tested on 25 (5 videos for each strain) 1-minute videos (30Hz). First, a trained human observer examined all videos to locate all foraging events. By applying the algorithm with α varying from 0 to 1, the performance result is shown as a receiver operating characteristic (ROC) curve [12] in Figure 5 and Table 1. We choose α = 0.5 because there is a sharp bend in the ROC curve there (at which point the True Positive fraction is over 93% while the False Positive fraction is less than 6%).

Table 1. The True Positive, True Negative, False Positive, and False Negative values for the ROC curve.

False Positive	True Positive	False Negative	True Negative	α
1.0000	0.9637	0.0363	0	0
0.7116	0.9609	0.0391	0.2884	0.1
0.4890	0.9554	0.0446	0.5110	0.2
0.3176	0.9491	0.0509	0.6824	0.3
0.1819	0.9442	0.0558	0.8181	0.4
0.0597	**0.9351**	**0.0649**	**0.9403**	**0.5**
0.0435	0.7901	0.2099	0.9565	0.6
0.0287	0.6820	0.3180	0.9713	0.7
0.0205	0.5941	0.4059	0.9795	0.8
0.0153	0.4986	0.5014	0.9847	0.9
0.0119	0.4010	0.5990	0.9881	1.0

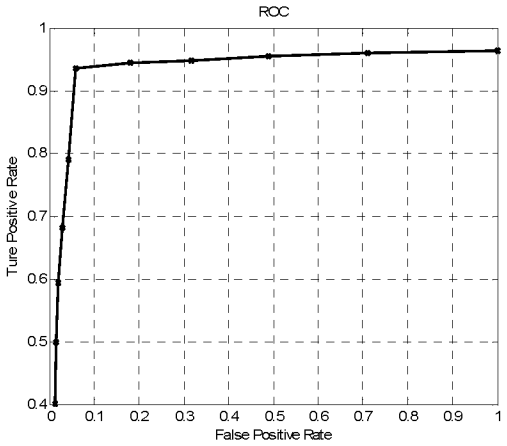

Figure 5. A plot of the receiver operating characteristic (ROC) curve with α varying from 0 to 1.

Statistical analysis of foraging events: After foraging events were detected for each strain, we extracted the following features from the bending curves from all detected events:

1) Wave amplitude: is defined to be the depth of nose bending (in degrees) during a foraging event. Once a foraging event is found, we compute {abs[SP-MP]+abs[EP-MP]}/2 to be its amplitude.

2) Time interval between adjacent foraging events: for adjacent events, this is the time interval between the end point EP of the first event and the start point SP of the second event.

3) Frequency of individual foraging event: this parameter represents the inverse of the period of an individual foraging event, which can be expressed as

Table 2. Foraging related features extracted from all events detected by the algorithm.

Mutant type	*dgk-1(nu62)*	*glr-1(n2361)*	*goa-1(n1143)*	*trpa-1(ok999)*	wild type
Total frames	34136	43728	32379	35010	36835
Total foragings	1669	1604	1820	1480	1789
Amplitude (AVE)	15.13	14.91	19.26	15.71	14.15
Amplitude (STD)	9.30	8.27	11.14	9.00	8.34
Interval (AVE)	0.199	0.386	0.171	0.249	0.216
Interval (STD)	0.245	0.465	0.206	0.325	0.293
Frequency (AVE)	4.51	4.31	4.00	4.19	4.57
Frequency (STD)	1.58	1.64	1.57	1.66	1.61
# of foraging in 10 seconds	14.67	11.00	16.86	12.68	14.57

1/T where T is the time length between the start point SP and the end point EP of the event.

The means and standard deviations of each feature were computed for each strain. The results are in Table 2. The first row shows the mutant type. The second row lists the total number of frames in which the worms were moving forward in the 30 videos of that strain. The third row shows the number of foraging events detected by the algorithm. The means and standard deviations of features are listed in rows 4 and 5 (waving amplitude), rows 6 and 7 (time interval between adjacent events) and rows 8 and 9 (the frequency of nose waving during foraging events).

We also computed the foraging rate, which is defined to be the number of foraging events within 10 seconds (300 frames), for each strain. The results are in Table 2 (row 10). Mutant types *dgk-1* and *goa-1* which are hyperactive for locomotion and foraging have higher foraging rate in 10 seconds whereas *glr-1* and *trpa-1* forage more slowly than wild type. Furthermore, wild type and *dgk-1* have very close foraging rate in 10 seconds, which matches the results in Table 2 that *dgk-1* and wild type have similar foraging behavior.

4. Conclusion

The main contributions of this paper can be summarized as follows: 1) we developed and tested a new algorithm for automatic detection of foraging events. 2) We provided quantitative analysis of foraging behavior, which has not previously been achieved, for several mutant types. 3) We verified the existence and quantified the amount of difference in the depth of nose bending between normal worms and lesioned or mutant animals, which was reported only anecdotally in previous studies. Previously, foraging events were scored by human observers which is tedious and labor-intensive. The development of automated methods for the study of foraging behaviors makes it possible to reliably detect foraging events and quantitatively parameterize foraging patterns. The algorithms we developed should have utility in future studies of foraging behavior.

References:

[1] J. White, E. Southgate, J. Thomson and S. Brenner, "The structure of the nervous system of the nematode *Caenorhabditis elegans", Phil Trans R Soc Lond (Biol)*, vol. 314, pp. 1-34, 1986.

[2] L. Avery and J. H. Thomas, *Feeding and defecation. C. elegans II*, Cold Spring Harbor, NY, 1997.

[3] W. F. Schafer, "Genetics of egg-laying in worms", *Annu Rev Genet*, vol. 40, pp. 487-509, 2006.

[4] M. Driscoll and J. Kaplan, "*Mechanotransduction. C. elegans II*", Cold Spring Harbor, NY, 1997.

[5] A. C. Hart, S. Sims and J. M. Kaplan, "Synaptic code for sensory modalities revealed by *C. elegans* GLR-1 glutamate receptor", *Nature*, vol. 378, pp. 82-85, 1995.

[6] L. Segalat, D. A. Elkes and J. M. Kaplan, "Modulation of serotonin-controlled behaviors by G_o in *Caenorhabditis elegans", Science*, vol. 267, pp. 1648-1651, 1995.

[7] S. Brenner, "The genetics of Caenorhabditis elegans", *Genetics*, vol. 77, pp. 71-94, 1974.

[8] W. Geng, P. Cosman, C. Berry, Z. Feng, and W. R. Schafer, "Automatic tracking, feature extraction and classification of *C. elegans* phenotypes", *IEEE Trans Biomed Eng*, vol. 51, pp. 1811-1820, 2004.

[9] R. Gonzalez and R. Woods, "*Digital Image Processing"*, 2nd ed. Prentice Hall, NJ, 2002.

[10] K. S. Kindt, V. Viswanath, L. Macpherson, K. Quast, H. Hu, A. Patapoutian and W. R. Schafer, "*Caenorhabditis elegans* TRPA-1 functions in mechanosensation", *Nat Neurosci,* vol. 10, pp. 568-577, 2007.

[11] K. Huang, P. Cosman and W. R. Schafer, "Machine vision based detection of omega bends and reversals in *C. elegans", J Neurosci Methods*, vol. 158, pp. 323-336, 2006.

[12] C. E. Metz, "Basic Principles of ROC Analysis", *Seminars in Nuclear Medicine*, vol. 8, no. 4, pp. 283-298, 1978.